Annals of Phytomedicine 14(1): 1028-1042, 2025

DOI: http://dx.doi.org/10.54085/ap.2025.14.1.103

Annals of Phytomedicine: An International Journal
http://www.ukaazpublications.com/publications/index.php

Print ISSN : 2278-9839 Online ISSN : 2393-9885

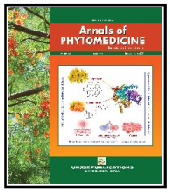

Orginal Article : Open Access

A comparative metabolome analysis of seed, root, and leaf of blackgram cultivars in response to Mungbean yellow mosaic virus (MYMV) infection reveals a unique signature profile for resistance

R. Sariga*, P. Renukadevi*, S. Nakkeeran◆, I. Yesuraja***, J. Ramalingam**, A. Yuvaraja**** and S. Vellaikumar****

** Department of Plant Pathology, Centre for Plant Protection Studies, Tamil Nadu Agricultural University, Coimbatore-641 003, Tamil Nadu, India*

*** Department of Plant Biotechnology, Centre for Plant Molecular Biology and Biotechnology, Tamil Nadu Agricultural University, Coimbatore-641 003, Tamil Nadu, India*

**** Department of Plant Pathology, Agriculture College and Research Institute, Madurai-625 107, Tamil Nadu, India*

***** National Pulse Research Centre, Vamban-622303, Pudukkottai, Tamil Nadu, India*

Article Info

Article history
Received 6 March 2025
Revised 23 April 2025
Accepted 24 April 2025
Published Online 30 June 2025

Keywords
Mash 1008
CO5
Myo-inositol
Arachidonic acid
Tryptophan metabolism
Fatty acid metabolism

Abstract

Yellow mosaic disease (YMD), caused by the Begomovirus *Vigna radiata* (Mungbean yellow *mosaic virus* (MYMV), is a significant threat to blackgram (Vigna mungo) production, leading to severe yield losses. This study presents a comparative metabolomic analysis of resistant (Mash 1008) and susceptible (CO_5) blackgram cultivars to uncover the biochemical basis of resistance and susceptibility to MYMV infection. Using gas chromatography-mass spectrometry (GC-MS), metabolite profiling was conducted on seeds, roots, and leaves of both cultivars under MYMV-infected conditions. Metabolome signatures of resistant (Mash 1008) and susceptible (CO_5) blackgram cultivars in response to MYMV infection displayed an altered metabolite profile in seed, root, and leaves. Resistant cultivars (RC) exhibited elevated levels of antiviral metabolites such as lactic acid, methyl linoleate, and arachidonic acid. In contrast, the susceptible cultivar (SC) was characterized by higher metabolites, including docosahexaenoic acid, fructofuranose, and chiro-inositol, associated with susceptibility pathways. Metabolite enrichment analysis (MSEA) of RC-Mash 1008 expressed the maximum abundance of galactose metabolism and unsaturated fatty acid biosynthesis, emphasizing their robust metabolic adaptability. Conversely, SC-CO5 had moderate enrichment in amino acid and carbohydrate metabolism, reflecting a weaker defense profile. This comparative analysis underscores the significance of targeted metabolites and pathways in enhancing resistance mechanisms, offering valuable insights for developing strategies to improve crop resilience. By decoding the metabolic secrets of resistance and susceptibility in blackgram cultivars, this study provides a promising avenue for developing innovative strategies to combat YMD, a step closer to securing global pulse production against viral threats.

1. Introduction

Blackgram (*Vigna mungo* (L.) Hepper) is an important leguminous crop cultivated for its protein-rich seeds. It is a highly prized pulse crop in South Asia due to its superior digestible protein content (25-26%), carbohydrates (60%), lipids (1.5%), minerals, amino acids, and vitamins (Jegadeesan *et al*., 2021). India is a leading producer and consumer of pulses, accounting for approximately 54% of global production and 17% of total land under cultivation (Singh *et al*., 2016; Gupta *et al*., 2021). The crop is also cultivated in Bangladesh, Pakistan, Myanmar, Sri Lanka, Thailand, Nepal, and Philippines. Due to biotic and abiotic stress, blackgram production in India has remained unpredictable throughout the last ten years. India produces about 2 million tons of blackgram from over 4 million hectares, with an average yield of 598 kg/ha during 2023-24 (Raghunadha Reddy, 2024). Blackgram farming faces major challenges due to the infection of yellow mosaic disease (YMD), which is responsible for the reduction of crop yield and quality.

In Tamil Nadu, YMD in various legumes is caused by *Begomovirus vignaradiata* (Mungbean yellow mosaic virus), which belongs to the genus *Begomovirus* of the family *Geminiviridae,* and it mainly infects various legume plants. YMD causes significant yield reduction in all blackgram (*V. mungo*) cultivars (Basak *et al*., 2005). Successful pathogenesis is accompanied by an elevated rate of anatomical and metabolic abnormalities, which results in the formation of bright yellow chlorotic patches on diseased leaves.

Among the various blackgram cultivars, Mash 1008 has gained prominence due to its resistance to MYMV. While CO5 is highly susceptible and exhibits severe symptoms, including widespread leaf yellowing and significant yield reduction (Rajalakshmi *et al*., 2024). Investigations on the diversity of metabolome profiles between these two cultivars provides valuable insights into the mechanisms of MYMV resistance and susceptibility. This differential analysis may additionally reveal the role of each plant organ in the metabolism

Corresponding author: Dr. S. Nakkeeran
Professor (Plant Pathology), Department of Plant Pathology, Tamil Nadu Agricultural University, Coimbatore-641 003, Tamil Nadu, India
E-mail: nakkeeranayya@tnau.ac.in
Tel.: +91-7598489226

of nutrients, secondary metabolites, and signalling biomolecules, providing us with insight into the plant's phenotypic features and resilience to environmental challenges.

Plant-pathogen interactions significantly alter cellular metabolism, resulting in changes to primary metabolites and the elicitation of defense genes (Kumudini *et al.,* 2018). Common plants contain bioactive compounds that enhance the immune system and provide protection against pests and diseases (Dhanushkodi *et al.,* 2024).

Secondary metabolites in plants are critical for various biological functions, enabling plants to adapt and survive even in adverse environmental conditions (Weng *et al*., 2021). Plant-derived substances such as curcumin derivatives, flavonoids, triterpenes, and alkaloids have shown potential antiviral activities (Vijai Selvaraj *et al.,* 2024). Exploring the substances and mechanisms behind plant-pathogen interactions is essential for unlocking plants' complex defensive strategies to protect themselves.

Metabolite profiling or metabolomics involves the systematic study of the small molecules (metabolites) present within an organism. In plants, metabolites play crucial roles in physiological processes, including growth, development, and defense against pathogens. Roots, stems and leaves play distinct roles in a plant's response to biotic stress. Although, plant-pathogen interactions have been explored at the biochemical and molecular levels (Peyraud *et al*., 2017), it is important to explore the knowledge of susceptible plant responses to infections in terms of intrinsic chemical variation and metabolic pathway modulations. This reprogramming involves changes to core metabolic pathways such as carbohydrates, amino acids, and lipids to satisfy the greater energy needs for pathogen growth and defense activation (Llave *et al*., 2016). The phytochemical defence system effectively protects and synthesizes complex compounds with unique stereochemistry and modes of action (Bhawana Sharma *et al.,* 2021). Gas chromatography-mass spectroscopy (GC-MS) is a precise analytical technology that detects compounds in extracts at low concentrations. It is particularly effective for identifying bioactive chemicals such nitro compounds, alcohols, acids, esters, alkaloids, steroids, and long-chain hydrocarbons (Narmadha Devi *et al.,* 2024). Species-specific exploration allows breeders to discover unique chemical profiles, leading to novel products with therapeutic benefits, and market demand. This promotes innovation and competitiveness in the food, pharmaceutical, and perfumery industries (Vaishnavi *et al.,* 2024).

The present investigation provides a comprehensive metabolomic analysis of different plant tissues: seeds, roots, and leaves from both resistant and susceptible blackgram cultivars. By examining the metabolite profiles across these tissues, we aim to unravel the signature of biomolecules conferring resistance to YMD resistance.

2. Materials and Methods

2.1 Inoculation of MYMV in blackgram cultivars

Seeds of resistant (Mash 1008) and susceptible (CO5) cultivars were collected from the National Pulse Research Centre (NPRC), Vamban, Pudukottai, Tamil Nadu, India. Seeds were sown and established in pot culture under glasshouse conditions. Plant samples exhibiting yellow mosaic symptoms were collected from the blackgram field (Department of Pulses, Tamil Nadu Agricultural University, Coimbatore). DNA was extracted from leaf samples using the CTAB method to confirm the presence of MYMV, and it was confirmed through PCR using coat-specific primers. The primers DNA A CPF (ATGGGKTCCGTTGTATGCTTG) and DNA A CP R (GGCGT CATTAG CATAGGCAAT), which would amplify a 1 kb amplicon of DNA A, were used to confirm MYMV. The PCR conditions are as follows: 94°C for 2 min of initial denaturation, 95°C for 1 min of denaturation, 55°C for 2 min of annealing, 72°C for 3 min of extension, and 10 min of final extension. The partial PCR products were sequenced availing the facility at Biokart Pvt Ltd, Bangalore. Further, the sequences were edited and submitted to the NCBI database. The MYMV positive symptomatic leaves were used for transmission studies.

Whiteflies reared in the insect-proof glass house at TNAU (*Bemisia tabaci*) were allowed to feed for 24 h acquisition access period (AAP) with 20 whiteflies per clip cage using only PCR-positive MYMV symptomatic leaf samples. Following AAP, whiteflies were given 24 h inoculation access period (IAP) to feed on healthy blackgram plants (Mash 1008 and CO5) at two primary leaf stage; three replications and four plants per replication were kept. Plants were maintained in insect-proof cages. After 24 h IAP, clip cages with whiteflies were removed and killed by spraying systemic insecticide (Imidacloprid 0.6% SC). The plants were observed for symptom expression. After 45 days of plant growth at the reproductive phase, seeds, roots and leaves were collected from the inoculated plants and healthy uninoculated control of both cultivars (60 DAS) to proceed further for GC-MS analysis to understand the diversity of biomolecules.

2.2 Sample preparation and metabolite extraction

Fresh samples (5 g) of seed, root and leaf from the resistant cultivar Mash 1008 and susceptible cultivar CO5 were frozen and homogenized using liquid nitrogen. From the homogenized sample, 0.3 g of powdered material was transferred into 2 ml tubes. Roughly 1.4 ml of 100% methanol was added and vortexed. Then, 50 µl (0.2 mg/ml) of ribitol was added to it. The resultant mixture was incubated for fifteen minutes at 70°C with continuous stirring and then centrifuged for 20 min at 4°C at 12,000 rpm. After transferring the supernatant to a 0.2 µm filter, 750 µl of chloroform and 1.4 ml of water was added. The mixture was mixed well and centrifuged at 12000 rpm for 10 min. 1 ml of the upper polar phase was transferred to new tubes, and the remaining 1 ml of supernatant was saved in another tube for future use. The upper phase was concentrated at 45°C using a vacuum concentrator for three hours. 50 µl of methoxamine hydrochloride (20 mg/ml of pyridine) was added to the supernatant fraction. The tubes were incubated in the sonicator for 2 h at 37°C while being constantly shaken. Subsequently, samples were incubated at 37°C for 30 min, after which 80 µl of N-methyl-N(trimethylsilyl) trifluoroacetamide (MSTFA) was added. Centrifuged for 3 min at 10,000 rpm. The supernatant was subsequently transferred to the vials for GC-MS analysis.

2.3 Untargeted GC-MS analysis and statistical analysis

Untargeted GC-MS analysis was performed to identify biochemical compounds in crude extracts from RC and SC samples. One microliter of each sample was injected into a TRACE™ GC Ultra system equipped with a DB-5MS column and a DSQII quadrupole mass spectrometer. Helium was used as the carrier gas with a flow rate of 1 ml/min. The oven temperature was initially set at 150°C and increased to 250°C at specific heating rates. Spectral data were processed using AMDIS for peak deconvolution, baseline adjustment, and retention time alignment. Metabolites were identified using the NIST library based on similarity indices.

2.4 Statistical analysis

For statistical analysis, data preprocessing included peak extraction, intensity detection, retention time correction, alignment, normalization, and handling of missing values. Processed data were log2-transformed and Pareto-scaled before being analyzed using MetaboAnalyst 5.0. Principal Component Analysis (PCA) was used to explore group differences, while KEGG pathway annotation and enrichment analysis were performed to classify metabolites by function. Univariate and multivariate statistical methods were applied to identify key metabolites distinguishing between biological conditions.

3. Results

The field collected leaf samples exhibiting yellow mosaic symptoms (Figure 1a) and seed samples from the infected plants were positive for MYMV-coat protein specific primers and the PCR products were sequenced (Figure 1b). The sequences were edited and analyzed. In BLAST search, the sequences exhibited 97 to 100 per cent identity with MYMV isolates with accession numbers, *viz*., MK409376 (Karnataka), MK409375 (Karnataka), PP470806 (Karnataka), PP539000 (Tamil Nadu) and PP738873 (Tamil Nadu). The sequences were submitted in NCBI and accession numbers were obtained (PV259945 and PV259946). PCR analysis thereby confirmed the presence of MYMV, which was used for further inoculation studies (Figure 1b).

The resistant cultivar Mash 1008 and susceptible variety CO5 were grown under pot culture conditions and MYMV was inoculated by whitefly transmission (Figures 1c, e). In CO5, tiny chlorotic mosaic specks symptom expression started at 12th DAT; there was no symptom expression in Mash 1008 and healthy control (CO5 and Mash 1008) till the end (60DAT). In PCR analysis, CO5 leaves and seeds were positive with an expected amplicon of 1 kb, whereas there was no amplification in CO5 roots, all the parts of Mash 1008 samples and samples collected from healthy controls of both CO5 and Mash 1008 (Figures 1d, f). Seeds, root and leaf samples from both inoculated and non-inoculated plants of cultivars (Mash 1008 and CO5) were collected 60 days after sowing (DAS) and subjected to GC-MS analysis to identify the key molecules responsible for resistance and susceptibility to MYMV.

Figure 1a: Yellow mosaic disease symptoms in blackgram.

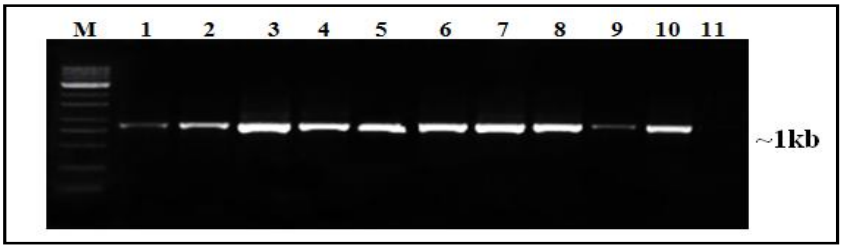

Figure 1b: Agarose gel electrophoresis of PCR products of DNA from blackgram leaf samples using MYMV CP primers. Lane M : 1 Kb ladder ; Lane 1, 2,3&4 : CO5 leaf;5,6,7,8: CO5 seed; Lane 9&10: Positive Control; Lane 11 : Negative control (Healthy leaf).

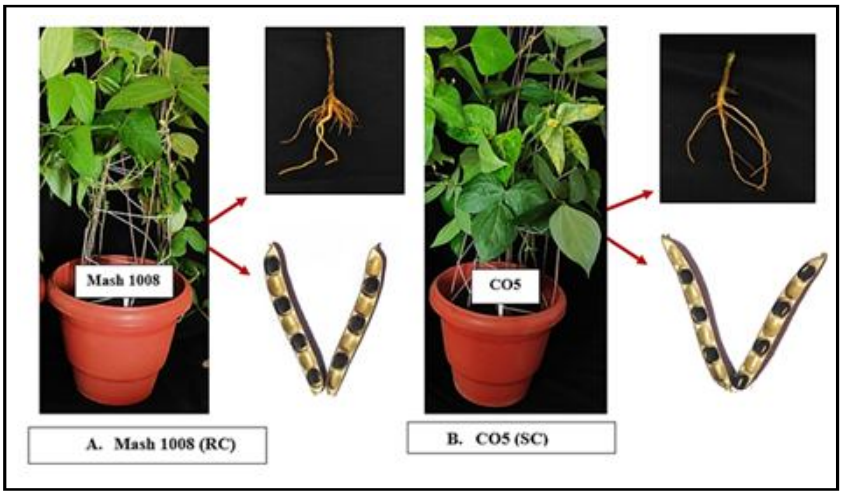

Figure 1c: Seed, root and leaves (MYMV transmitted) used in GC-MS study.

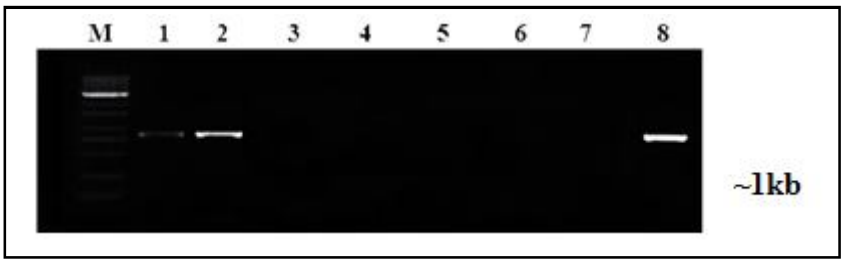

Figure 1d: Agarose gel electrophoresis of PCR products of DNA extracted from symptomatic leaf samples using MYMV CP primers. Lane M : 1 Kb ladder ; Lane 1: CO5 leaf; Lane 2: CO5 seed; Lane 3: CO5 root; Lane 4: Mash 1008 leaf ; Lane 5: Mash 1008 seed; Lane 6: Mash 1008 root; Lane 7: Negative control; Lane 8: Positive control.

Figure 1e: Seed, root and leaves (Healthy control) used in GC-MS study.

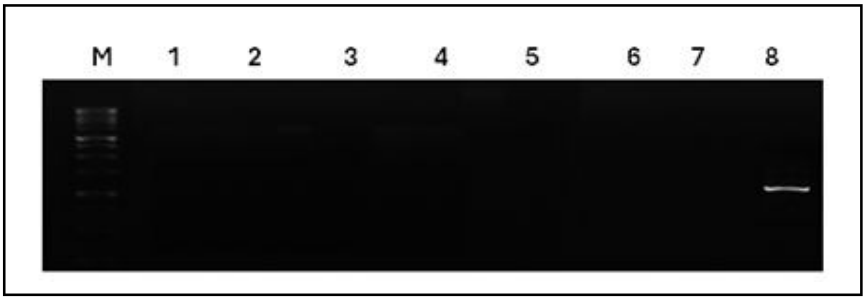

Figure 1f: Agarose gel electrophoresis of PCR products of DNA extracted from healthy leaf samples using MYMV CP primers. Lane M : 1 Kb ladder ; Lane 1: CO5 leaf; Lane 2: CO5 seed; Lane 3: CO5 root; Lane 4: Mash 1008 leaf ; Lane 5: Mash 1008 seed; Lane 6: Mash 1008 root; Lane 7: Negative control; Lane 8: Positive control.

In the current investigation, methanolic extracts of MYMV transmitted CO5 (SC) and Mash 1008 (SC) blackgram cultivars were analyzed using a GC-MS system to generate chromatographic and MS profiles of the samples. The gas chromatography data indicated the presence of various compositions of chemical compounds in the seeds, roots, and leaves of Mash 1008 and CO5.

3.1 Identifying unique biomolecules from different plant parts of resistant and susceptible blackgram cultivars

3.1.1 Seed

The healthy RC-Mash 1008 seeds were found to contain unique metabolites such as campestrol, rhamnose, asperuloside, hentriacontanoic acid, pyroglutamic acid, methyl myristoleate, stearic acid, dodecanol, gamma-sitosterol, and neophytadiene. In contrast, seeds of Mash 1008 infected with MYMV exhibited distinct compounds including ascorbic acid, dihydroglutamic acid, neronine, enolide, meadowlactone, amberin, and ressinamine. Similarly, CO5 seeds showed the presence of specific metabolites such as statine, uredіopropionic acid, metoprolol, mandelic acid, nicotinic acid, lauric acid, elaidic acid, cinnamic acid, linocinnamarin, and oleic acid. Moreover, MYMV-infected CO5 seeds displayed unique compounds like pyrrolidine, gliotoxigenin, oleic acid, 2-myristoyl pantothenic acid, and fenretinide (Figures 2a, c).

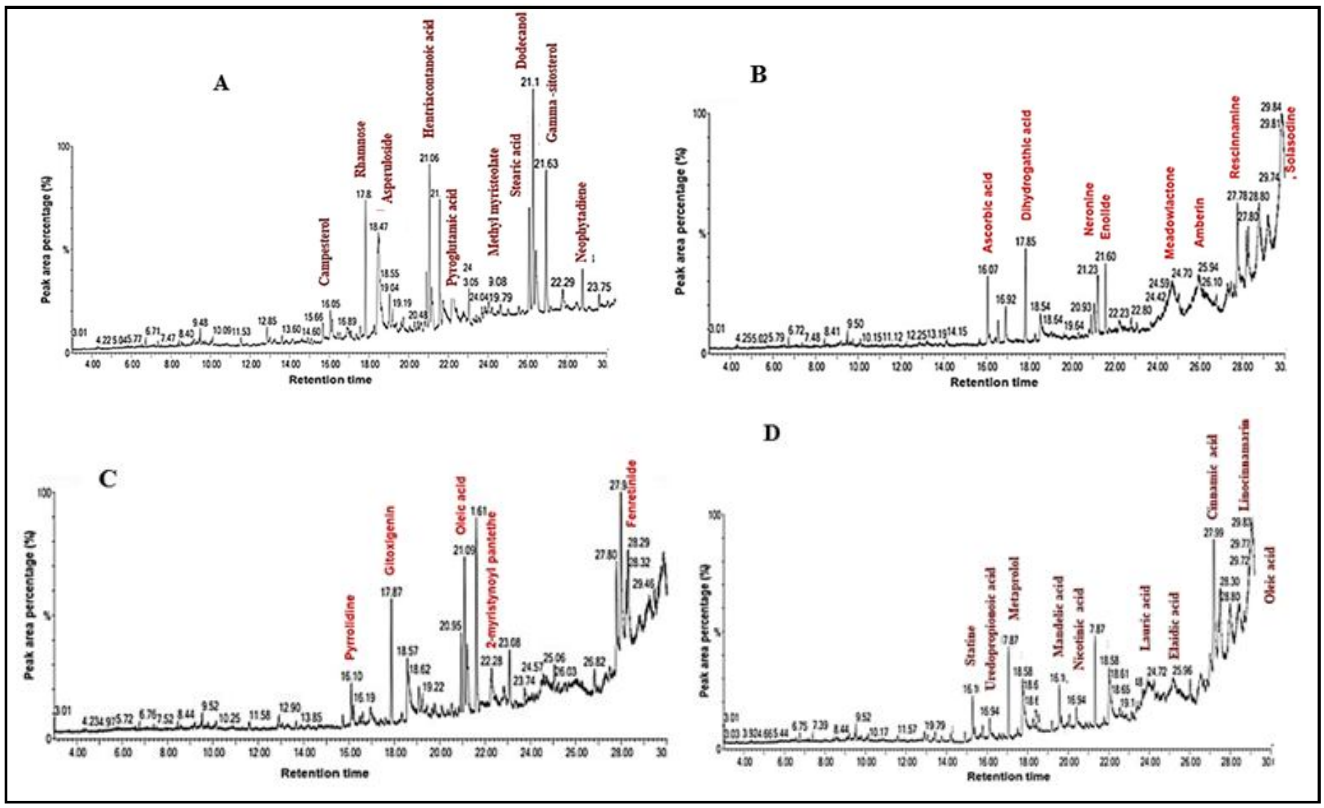

Figures 2a: GC-MS chromatogram of metabolites obtained from seed. A. Mash 1008 healthy seed, B. MYMV transmitted Mash 1008 seed, C. CO5 healthy seed, and D. MYMV transmitted CO5 seed.

The Venn diagram illustrated the distribution and overlap of elements among four groups: healthy control CO5 (HC (blue)), MYMV-transmitted CO5 (MC (yellow)), healthy control Mash 1008 (HM (green)), and MYMV-transmitted Mash 1008 (MM (red)). The MM group were found to contain the highest number of unique elements with 45 (20.6%), followed by HC with 43 (19.7%), HM with 34 (15.6%), and MC with 32 (14.7%). A small number of elements were shared exclusively between two groups, such as 12 elements (5.5%) between MC and HM, 13 (6%) between MC and MM, and 9 (4.1%) between HM and MM. Elements shared among three groups include 7 (3.2%) common to HC, MC, and HM; 9 (4.1%) to MC, HM, and MM; while only 4 elements (1.8%) are common across all four groups (Figure 2b).

3.1.2 Root

The GC-MS chromatogram analysis of root metabolites showed unique compounds in each sample. In the Mash 1008 healthy root (Figure 2c , A), unique compounds identified were lactic acid, glycerol, picose, tagatose, chiro-inositol, di-butyl-phtalate, glucose, sucrose, 3-hydroxyvaleric acid, pimelic acid, succinic acid and juniperic acid. In the MYMV-transmitted Mash 1008 root (Figure 2c,B), the unique molecules observed were bromotetradecane, methyl oleate, urocanic acid, theophylline, lauric acid, 3-hydroxyvaleric acid, cysteine and 3,4-methylglutaconic acid. The CO5 healthy root (Figure 2c, C) contained distinctive compounds such as lactic acid, acetic acid ethyl ester, glycerol, malic acid, dihydrouracil, citric acid, glutamic acid, hippuric acid, adonitol, chiro-inositol, sucrose,3-hydroxyvaleric acid and linocinnamarin. In the MYMV-transmitted CO5 root (Figure 2c,D), the unique metabolites were 2-amino-2-cyclopentylacetic acid, malonic acid, L-proline, 2-butenendioic acid, meso-erythritol, L-5-oxyproline, tartaric acid, xylitol, citric acid, ribonic acid, hippuric acid and fumaric acid.

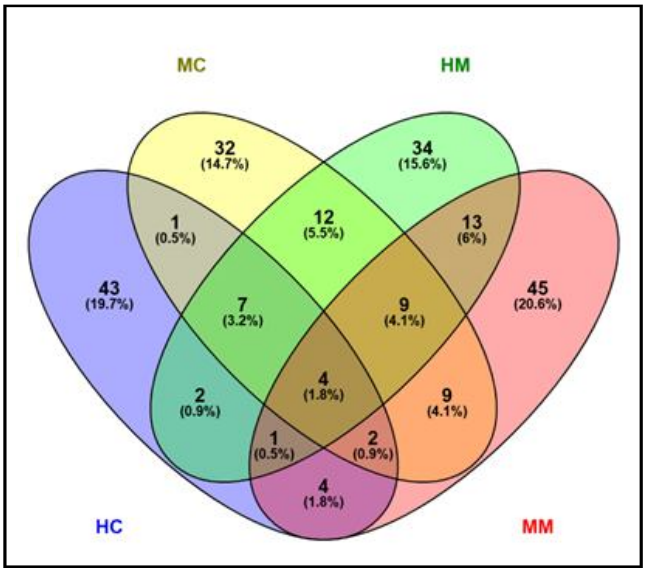

Figure 2b: Venn diagram showing the distribution of biomolecules in seeds between CO5 seed (CS) and Mash 1008 seed (MS). Healthy control CO5 (HC (blue)), MYMV-transmitted CO5 (MC (yellow)), Healthy control Mash 1008 (HM (green)), and MYMV-transmitted Mash 1008 (MM (red)).

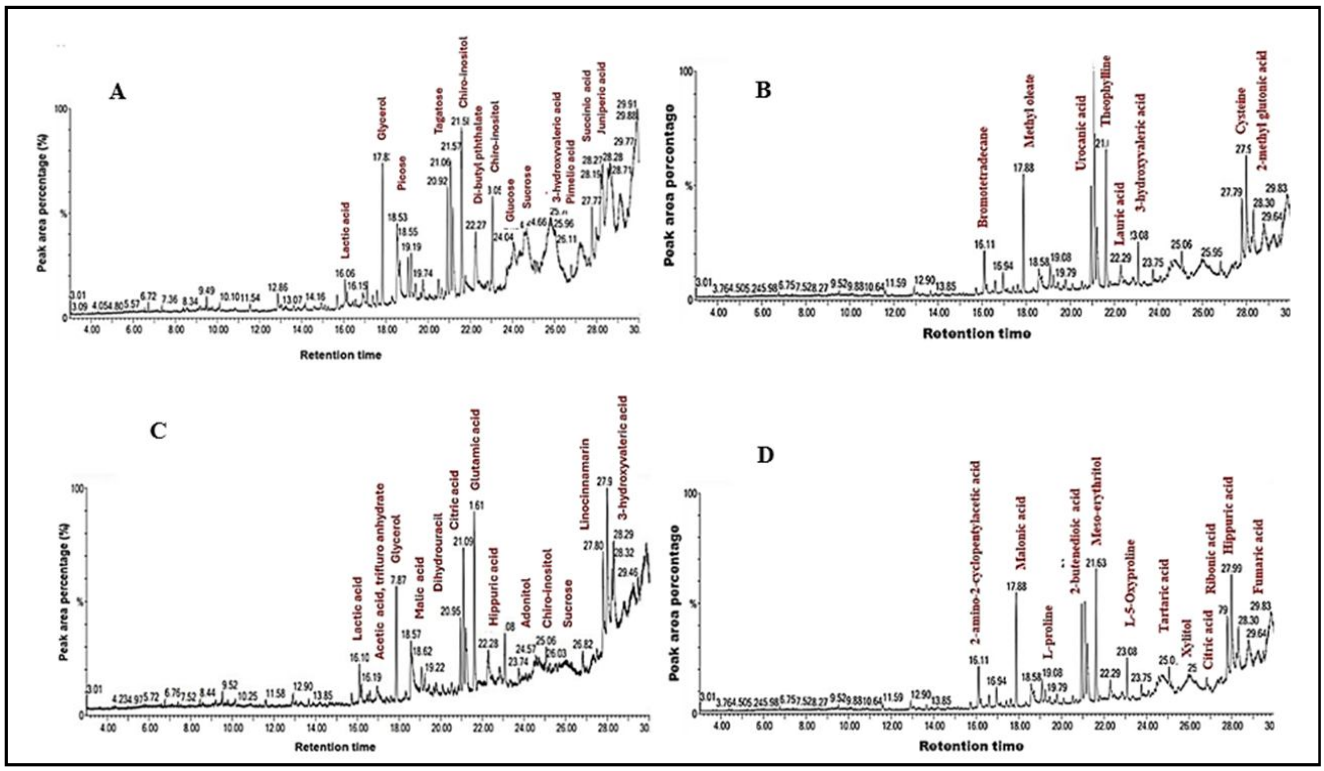

Figures 2c: GC-MS chromatogram of metabolites obtained from the root. A. Mash 1008 healthy root, B. MYMV transmitted Mash 1008 root, C. CO5, healthy root, and D. MYMV transmitted CO5 root.

The Venn diagram shown illustrates the distribution of elements across four different groups: healthy control CO5 (HC (blue)), MYMV-transmitted CO5 (MC (yellow)), healthy control Mash 1008 (HM (green)), and MYMV-transmitted Mash 1008 (MM (red)). The MC group held the highest number of unique elements with 71 (32.1%), followed by HM with 44 (19.9%), MM with 39 (17.6%), and HC with 20 (9%), indicating substantial distinctiveness within each group, particularly MC. Elements shared exclusively between two groups include 11 (5%) between HC and MC, 6 (2.7%) between HM and MM, 8 (3.6%) between MM and MC, and smaller overlaps such as 3 (1.4%) between HC and MM, and 2 (0.9%) between HC and MC.

Among three-group overlaps, 7 elements (3.2%) were common to HC, MC, and HM, while 3 elements (1.4%) were shared among HC, MC, and MM. Only 3 elements (1.4%) were shared among all four groups (HC, MC, HM, and MM), suggesting a low level of complete overlap (Figure 2d).

3.1.3 Leaf

The GC-MS chromatogram analysis of leaf metabolites revealed several unique compounds across the samples. In the Mash 1008 healthy leaves (Figure 2e, A), unique metabolites included isosorbide, palmitic acid, glutaconic acid, oleic acid, linoleic acid, glucose, and chlorogenic acid. In the MYMV-transmitted Mash 1008 leaves (Figure 2e, B), distinct compounds identified were tryptophan, linolenic acid, methyl succinate, glyceryl monooleate, dodecanol, cholesterol, and ribose. The CO5 healthy leaves (Figure 2e, C) showed the presence of isosorbide, palmitic acid, gluconic acid, hippuric acid, glucose, chlorogenic acid, and citric acid. Meanwhile, the MYMV-transmitted CO5 leaves (Figure 2e, D) contained unique molecules such as tryptophan, lactic acid, formic acid, 3-hydroxybutanoic acid, dodecanal, hexadecenoic acid, stearic acid, and hexitol glycoside.

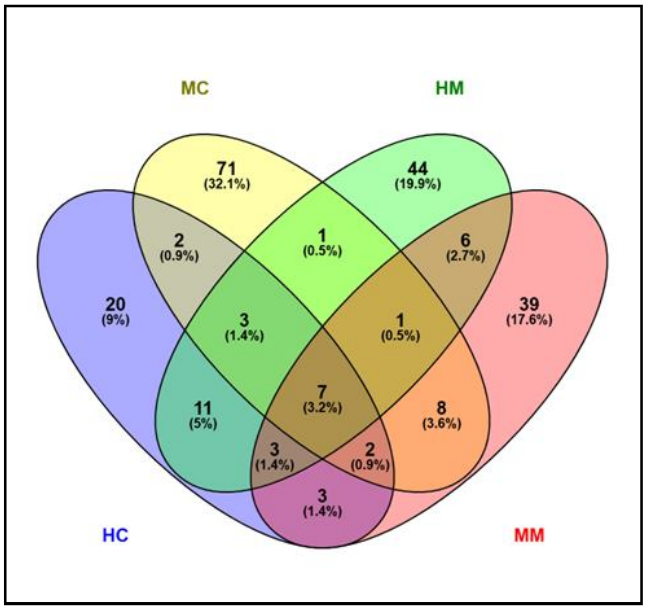

Figure 2d: Venn diagram showing the distribution of biomolecules between CO5 root and Mash 1008 root. Healthy control CO5 (HC (blue)), MYMV-transmitted CO5 (MC (yellow)), Healthy control Mash 1008 (HM (green)), and MYMV-transmitted Mash 1008 (MM (red)).

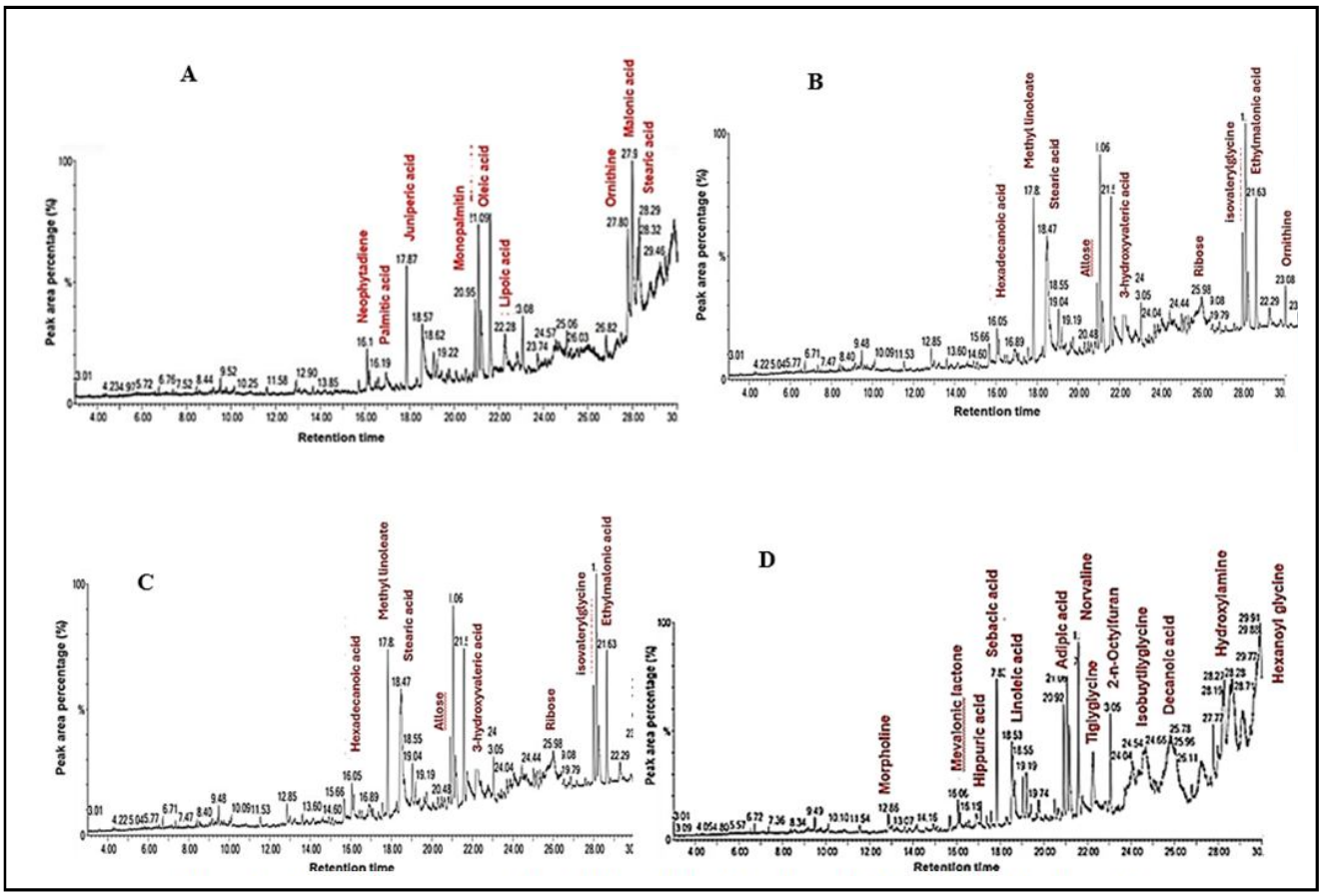

Figures 2e: GC-MS chromatogram of metabolites obtained from leaves. A. Mash 1008 healthy leaves, B. MYMV transmitted Mash 1008 leaves, C. CO5 healthy leaves, and D. MYMV transmitted CO5 leaves.

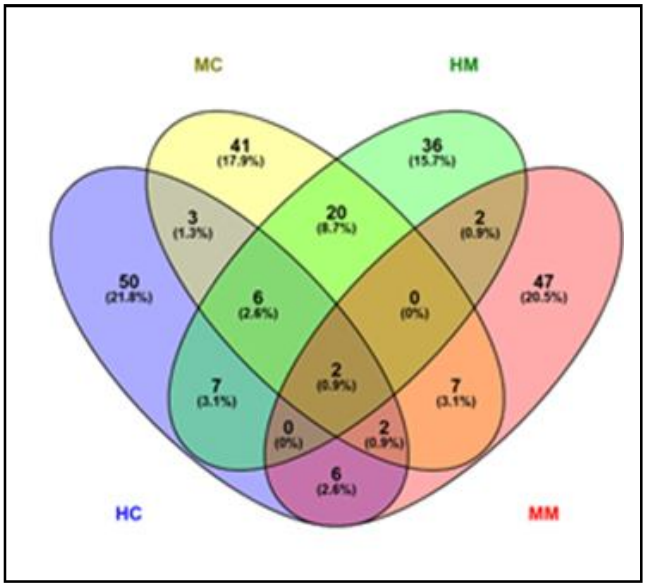

Figure 2f: Venn diagram showing the distribution of biomolecules in between leaves of CO5 and Mash 1008. Healthy control CO5 (HC (blue)), MYMV-transmitted CO5 (MC (yellow)), Healthy control Mash 1008 (HM (green)), and MYMV-transmitted Mash 1008 (MM (red)).

The Venn diagram illustrated the distribution and overlap of elements among four groups: healthy control CO5 (HC (blue)), MYMV-transmitted CO5 (MC (yellow)), healthy control Mash 1008 (HM (green), and MYMV-transmitted Mash 1009 (MM (red)). The highest number of unique elements were observed in the HC group with 50 elements (21.8%), followed by MM with 47 (20.5%), MC with 41 (17.9%), and HM with 36 (15.7%), indicating that each group contains a substantial portion of distinct elements. The most significant overlap was observed between MC and HM, which share 20 elements (8.7%), suggesting some level of similarity or interaction between these two groups. Smaller overlaps existed between HC and HM (7 elements, 3.1%), HC and MC (6 elements, 2.6%), and HC and MM (6 elements, 2.6%). Minimal overlaps were also seen between HM and MM (2 elements, 0.9%) and MC and MM (2 elements, 0.9%). Three-group overlaps included 6 elements (2.6%) shared by HC, MC, and HM, and 2 elements (0.9%) shared by HC, MC, and MM. Notably, there were no elements shared across all four groups, indicating a complete absence of universal commonality (Figure 2f).

3.2 Multivariate PCA biplot analysis highlights metabolomic divergence among resistant (Mash 1008) and susceptible (CO5)

The PCA biplot visualized the metabolic differentiation among four sample groups - HC (Healthy control CO5), HM (Healthy control

Mash 1008), MC (MYMV-infected CO5), and MM (MYMV-infected Mash 1008) based on principal component analysis. Each group was distinctly clustered, indicating clear differences in their metabolite profiles. The biplot also illustrated the influence of individual metabolites, represented by black arrows, on the separation of groups. Each colored dot represented a biological replicate, and the ellipses denote the 95% confidence intervals for each group, reflecting the clustering and variability within each treatment.

3.2.1 Seed

The first two principal components (PC1 and PC2) together explained a significant proportion of the total variance in the data, accounting for 39.1% and 34.51%, respectively. MC and MM groups exhibited tight clustering, suggesting low within-group variability, while HC and HM groups showed broader dispersion, reflecting greater internal variability. Metabolites like docosahexaenoic acid and rosiridin were more associated with the HC group, while glycerol, fructofuranose, and myo-inositol were more aligned with the MM group. Meanwhile, batyl alcohol, 7-hydroxyoctanoic acid, and methyl arachidonate contributed more significantly to the HM group. Central metabolites such as juniperic acid, ucidin, and luteolin appeared to have balanced contributions across the groups (Figure 3a).

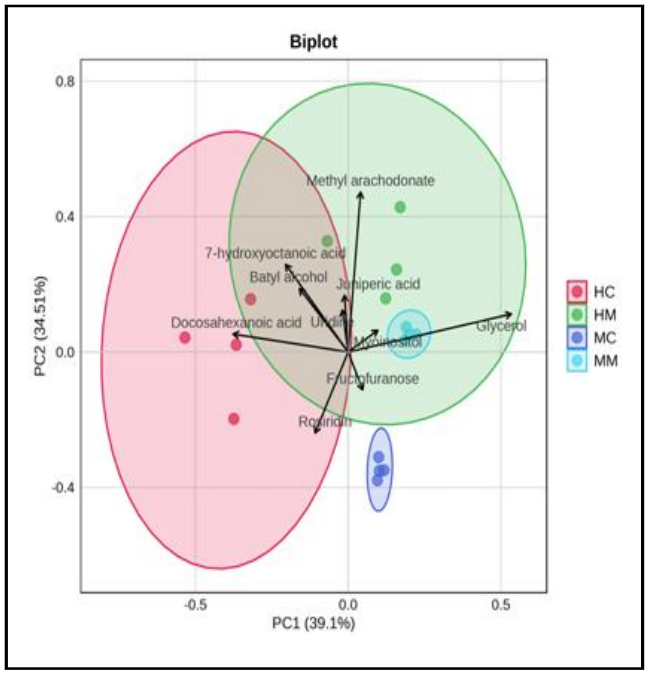

Figure 3a: PCA biplot showing seed metabolite-based separation among four groups. Arrows represent metabolites, with direction and length indicating their contribution to group separation. Ellipses show 95% confidence intervals. Healthy control CO5 (HC (blue)), MYMV-transmitted CO5 (MC (yellow)), Healthy control Mash 1008 (HM (green)), and MYMV-transmitted Mash 1008 (MM (red)).

3.2.2 Root

The x-axis (PC1) accounted for 84.61% of the total variance, while the y-axis (PC2) explained 6.13%, together capturing over 90% of the observed variation. The distribution of samples showed a clear separation between HC and HM groups, indicating distinct metabolomic shifts upon microbial treatment. The MM and MC groups appeared in close proximity but are slightly distinct, with MM tending toward the HM cluster, suggesting a partial restoration or modulation of the metabolic profile under microbe treatment during MYMV infection. Notably, metabolites such as glycerol, batyl alcohol, and valproic acid were more associated with the HC group, whereas docosapentaenoic acid, alpha-linolenic acid, and cysteine were aligned more closely with the HM group (Figure 3b).

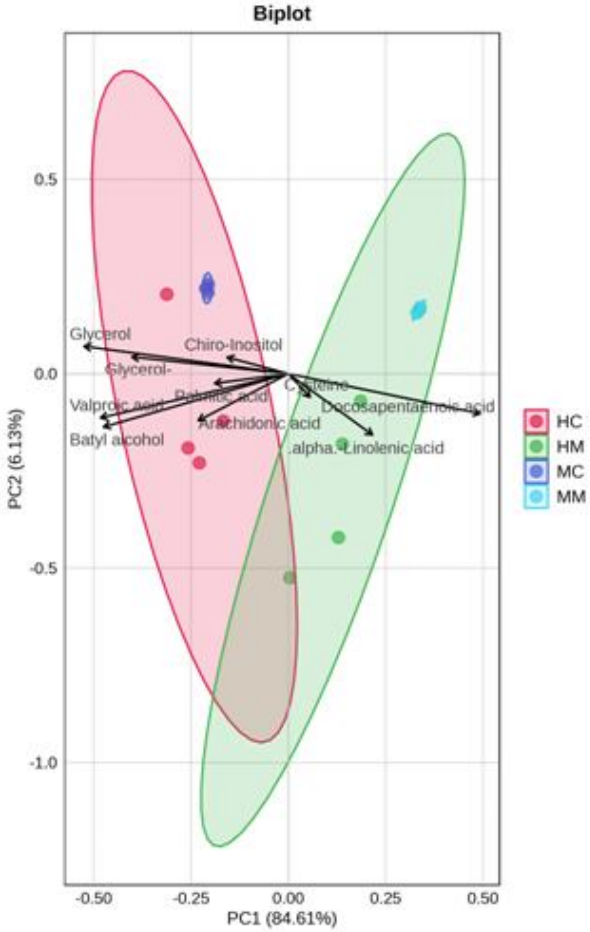

Figure 3b: PCA biplot showing root metabolite-based separation among four groups. Arrows represent metabolites, with direction and length indicating their contribution to group separation. Ellipses show 95% confidence intervals. Healthy control CO5 (HC (blue)), MYMV-transmitted CO5 (MC (yellow)), Healthy control Mash 1008 (HM (green)), and MYMV-transmitted Mash 1008 (MM (red)).

3.2.3 Leaf

The first principal component (PC1) explained 58.04% of the variance, while the second principal component (PC2) accounted for 21.18%. Metabolites such as beta-sitosterol, batyl alcohol, and lipoic acid were associated with the HC group, while HM was linked with compounds like 1,6-anhydroglucose and 3-methyladipic acid. Ribose and 6-octadecenoic acid were associated with the MM group (Figure 3c).

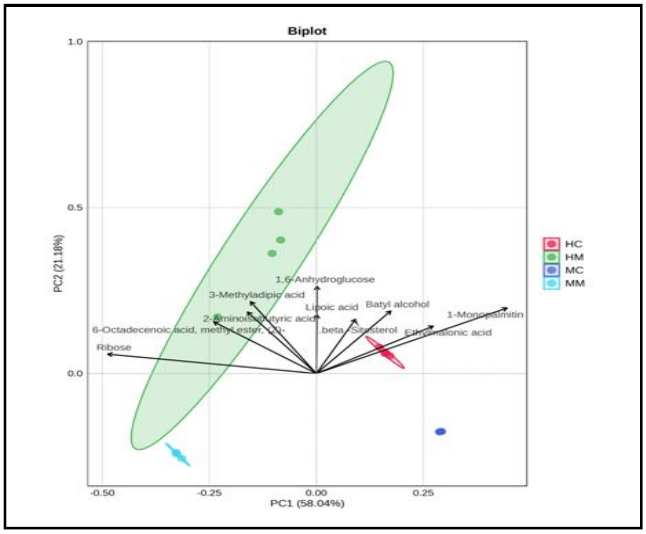

Figure 3c: PCA biplot showing leaf metabolite-based separation among four groups. Arrows represent metabolites, with direction and length indicating their contribution to group separation. Ellipses show 95% confidence intervals. Healthy control CO5 (HC (blue)), MYMV-transmitted CO5 (MC (yellow)), Healthy control Mash 1008 (HM (green)), and MYMV-transmitted Mash 1008 (MM (red)).

3.3 Comparative hierarchical clustering of metabolomic signatures in blackgram subjected to MYMV infection

The heatmap illustrated the hierarchical clustering of metabolite profiles across four treatment groups: HC (Healthy control CO5), HM (Healthy control Mash 1008), MC (MYMV infected CO5), and MM (MYMV infected Mash 1008). Each row represented a specific metabolite, while each column indicated a biological replicate. The colour gradient ranged from green (low abundance) to red (high abundance), indicating the relative abundance of each metabolite across the samples. The clustering of metabolites and samples reflected variations in metabolic profiles influenced by treatment type**.** Both metabolites and samples were clustered using hierarchical algorithms to reveal treatment-specific metabolic signatures and group-wise variations in metabolomic profiles.

3.3.1 Seed

Juniperic acid, 7-hydroxyoctanoic acid, and methyl arachidonate exhibited higher levels in HC and HM samples. Similarly, docosahexaenoic acid and uridine also show increased abundance in these two groups. In contrast, glycerol and myoinositol were predominantly enriched in the MC and MM classes. Chiroinositol and fructofuranose were also more abundant in MC and MM samples (Figure 4a).

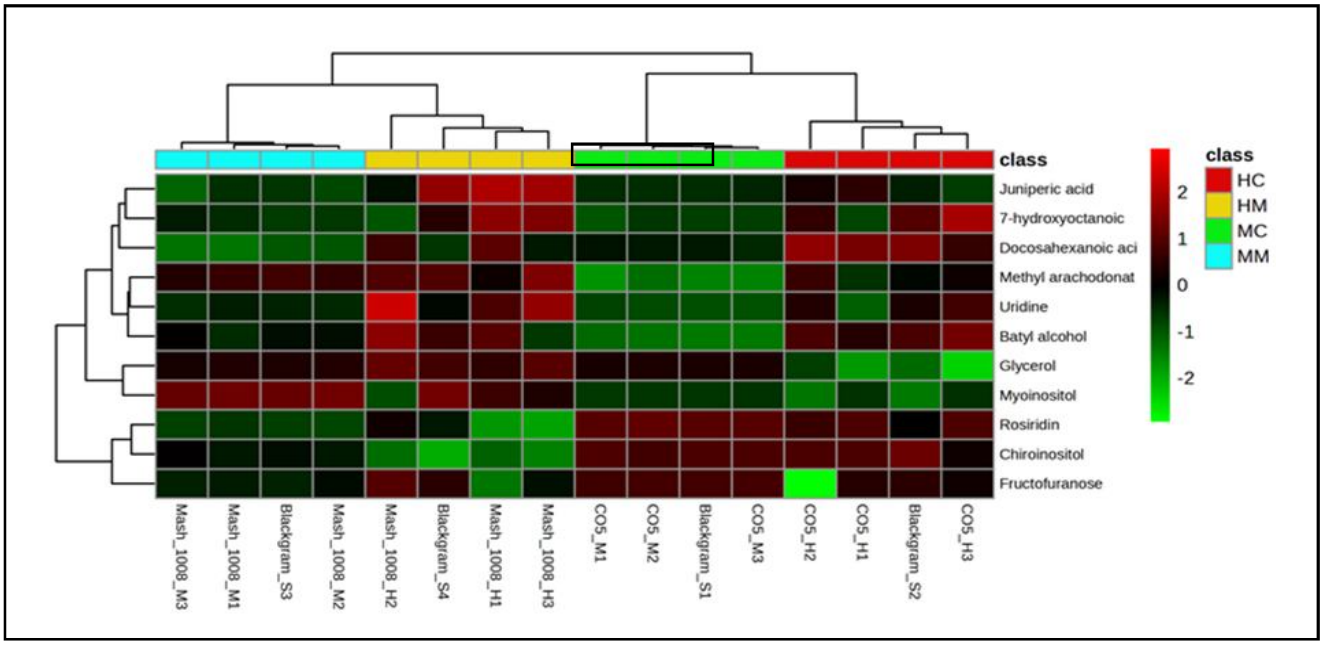

Figure 4a: Hierarchical clustering heatmap illustrating the relative abundance of identified metabolites in seeds of blackgram across four treatment groups: HC (Healthy Control: CO5), HM (Healthy Control: Mash 1008), MC (MYMV infected CO5), and MM (MYMV infected Mash 1008).

3.3.2 Root

Valproic acid, batyl alcohol, palmitic acid, and arachidonic acid were highly abundant in HC samples while showing lower intensities in HM, MC, and MM. Chiro-inositol and glycerol exhibited moderate abundance across most samples but were lower in MM. Myo-inositol and docosapentaenoic acid displayed high abundance in HM, particularly in Mash 1008 H3 and H2, while being less prevalent in MC and MM. Alpha-linolenic acid and cysteine were also elevated in HM samples compared to the others. Overall, HM samples showed distinct metabolite profiles with relatively higher levels of beneficial compounds compared to infected or other healthy varieties (Figure 4b).

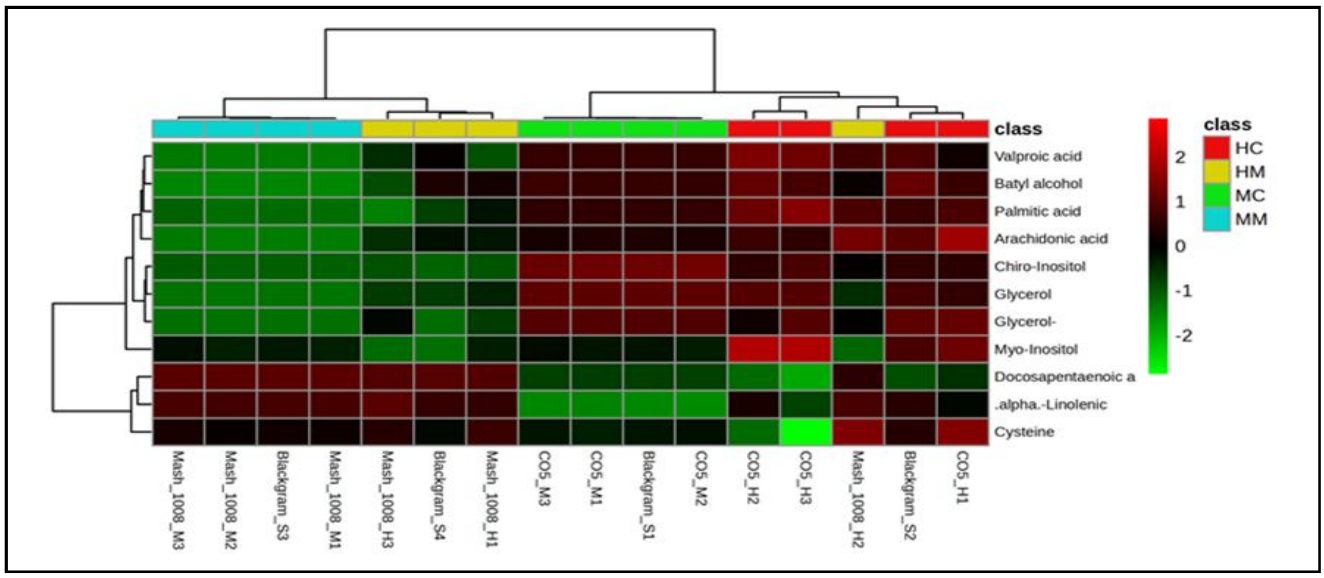

Figure 4b: Hierarchical clustering heatmap illustrating the relative abundance of identified metabolites in root of blackgram across four treatment groups: HC (Healthy Control: CO5), HM (Healthy Control: Mash 1008), MC (MYMV infected CO5), and MM (MYMV infected Mash 1008).

3.3.3 Leaf

The HM group showed higher intensities for metabolites such as eicosane, phenol 2,4-bis (1,1-dimethylethyl), chiro-inositol, D-pinitol, stigmasterol, and 1,6-anhydroglucose. Similarly, the MM group displays increased levels of compounds like 3-Methyladipic acid, docosenamide, 2-aminoisobutyric acid, and ethylmalonic acid. In contrast, the HC and MC groups showed relatively lower levels of several metabolites, including ribose, batyl alcohol, stearic acid, and hexadecanoic acid. Sterol-related metabolites such as β-Sitosterol and phytol showed distinct clustering patterns among the groups (Figure 4c).

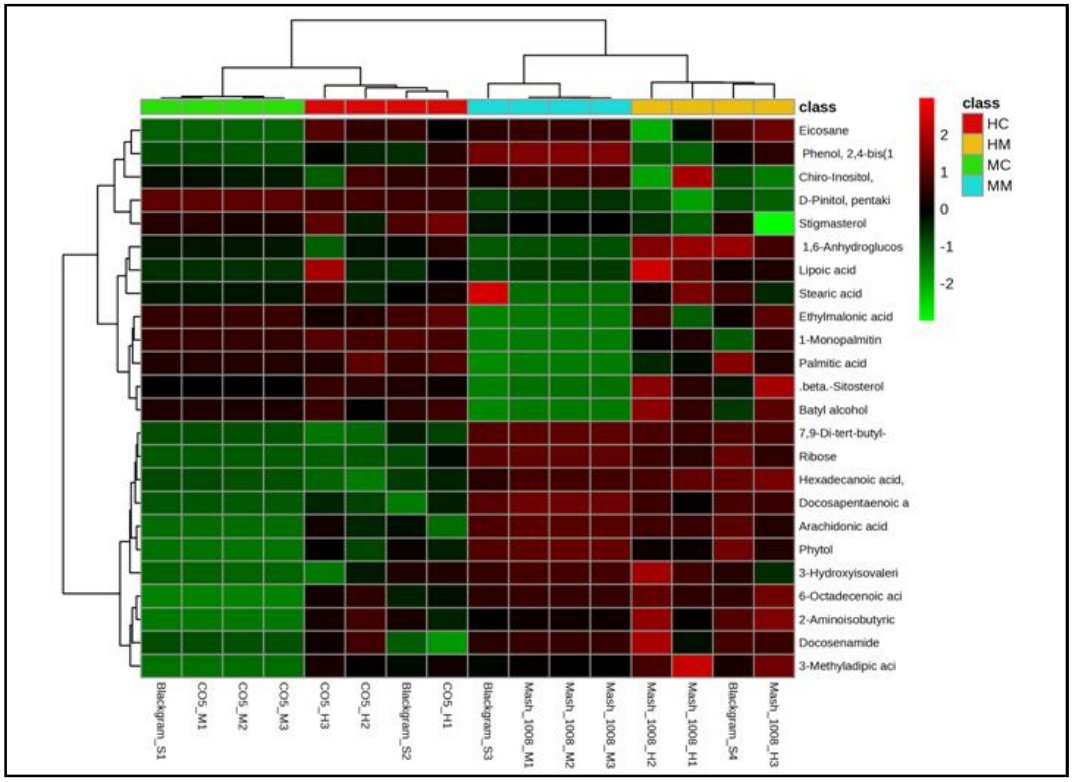

Figure 4c: Hierarchical clustering heatmap illustrating the relative abundance of identified metabolites in leaves of blackgram across four treatment groups: HC (Healthy Control: CO5), HM (Healthy Control: Mash 1008), MC (MYMV infected CO5), and MM (MYMV infected Mash 1008).

3.4 Decoding metabolic pathways: Top targets from enrichment analysis (MSEA)

Several key metabolic pathways were identified by metabolite enrichment analysis of susceptible cultivar CO5 and resistant cultivar Mash 1008 seed, root, and leaf samples. The *p*-value indicated the statistical significance of pathway enrichment and was represented by the colour gradient. Dark red emphasized the most important pathways ($p \approx 7\times10^{-4}$), indicating significant physiological need and enrichment. Orange to yellow bars represented pathways of moderate significance ($p \approx 2\times10^{-1}$), suggesting a possible need for further assessment. The least significant pathways ($p \approx 5\times10^{-1}$) were represented by white or light-colored bars, which are also less likely to be biologically significant. Pathways with red or orange bars were chosen for further study because lower *p*-values (darker colours) showed higher levels of enrichment, while lighter-colored pathways were usually deprioritized.

Lipid-related pathways including pyrimidine metabolism (~10, ~9e-04) and unsaturated fatty acid biosynthesis (~12, ~9e-04) were highly prominent in CO5 seed. Tryptophan metabolism was less significant (~2, ~4e-01), whereas amino acid pathways like alanine, aspartate, and glutamate metabolism had moderate enrichment (~6, ~2e-01) (Figure 5a).

In Mash 1008 seeds, the biosynthesis of unsaturated fatty acids had a *p*-value of ~2e-07 and an enrichment ratio of ~20. This was followed by the metabolism of galactose and linoleic acid (~15, ~2e-07). Ascorbate and aldarate metabolism were pathways of intermediate significance (~10, ~3e-01), whereas arachidonic acid metabolism showed lower enrichment (~5, ~5e-01) (Figure 5b).

The most significant pathways in the CO5 root were associated with the biosynthesis of unsaturated fatty acids and the metabolism of galactose (*p*-values <2e-04), with fatty acid biosynthesis and arginine making additional contributions. Significant enrichment was seen in energy pathways like the pentose phosphate and citrate cycles as well as pathways related to the metabolism of carbohydrates (such as the metabolism of starch and sucrose). On the other hand, there was significant enrichment in amino acid pathways such as the metabolism of alanine, aspartate, and glutamate (Figure 5c). In Mash 1008 root, the pathways for linoleic acid metabolism and unsaturated fatty acid production exhibited the highest *p*-values and enrichment ratios, which were about 7×10^{-7}. Other pathways showed minor enrichment with reasonably significant p-values, including the generation of pantothenate and coenzyme A and the metabolism of galactose. Large *p*-values for lower-ranked pathways, like cytochrome P450-mediated drug metabolism and steroid hormone synthesis, showed little enrichment (Figure 5d).

Highly enriched pathways in CO5 leaves, including fatty acid biosynthesis, galactose metabolism, and unsaturated fatty acid biosynthesis (enrichment ratios up to ~15, *p*-values <1e-04), were highlighted for their critical functions. The lipid and energy metabolism pathway, including glycerolipid metabolism and glycolysis/ gluconeogenesis, had moderate enrichment values (*p*-values ~2e-01 to ~5e-01) (Figure 5e).

In Mash 1008 leaves, lipid metabolism dominated with pathways such as fatty acid biosynthesis with the highest enrichment ratios (~15-20, *p*-values <1e-05). Key energy-related pathways, such as linoleic acid metabolism and fatty acid elongation emphasized their roles in energy storage and membrane dynamics, while moderate enrichment in pathways such as the pentose phosphate pathway highlighted energy production (Figure 5f).

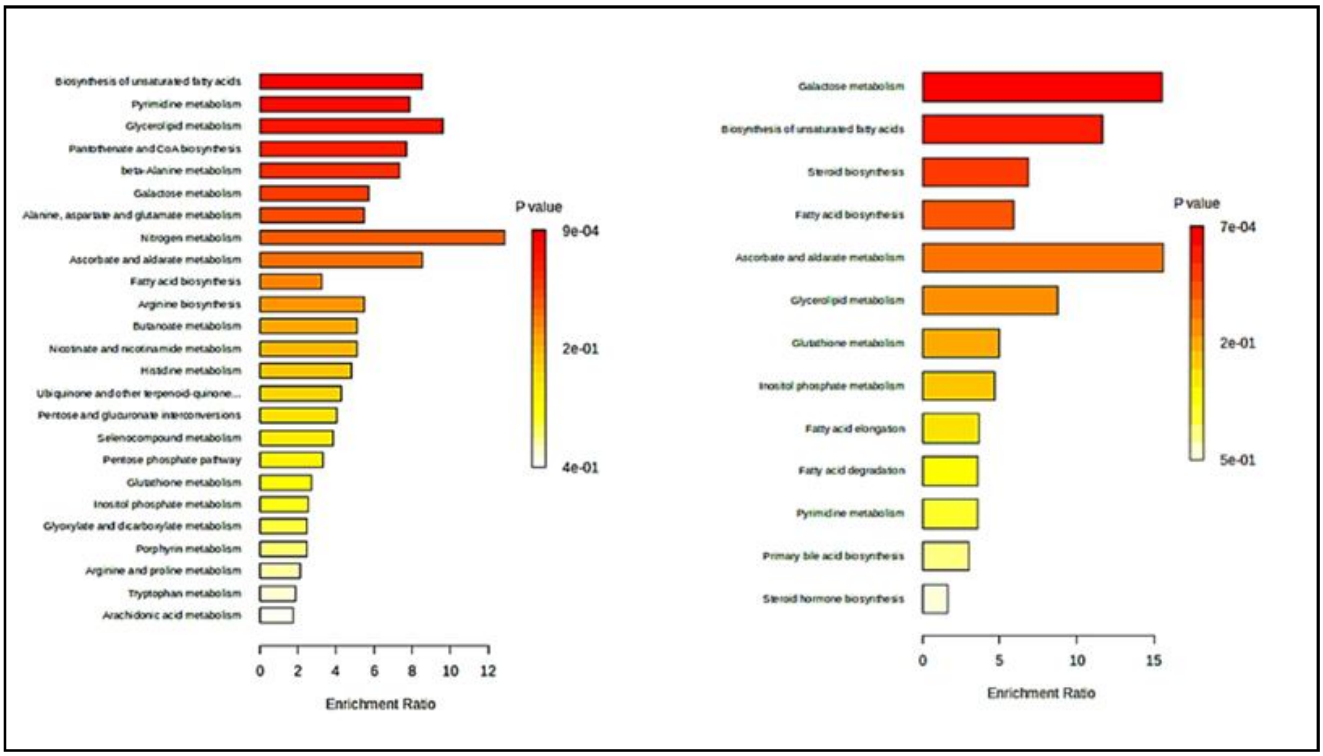

Figure 5a: Metabolic enrichment pathway analysis of CO5 seed; 5b: Metabolic enrichment pathway analysis of Mash 1008 seed.

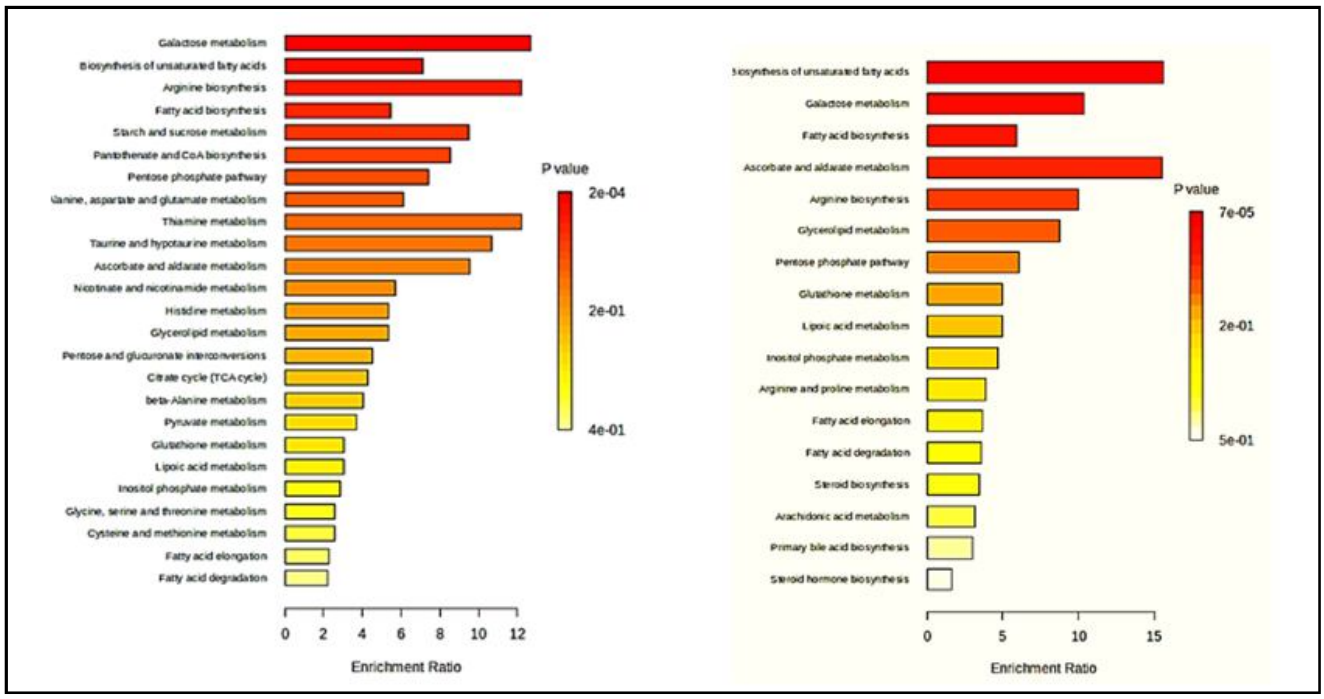

Figure 5c: Metabolic enrichment pathway analysis of CO5 root; 5d: Metabolic enrichment pathway analysis of Mash 1008 root.

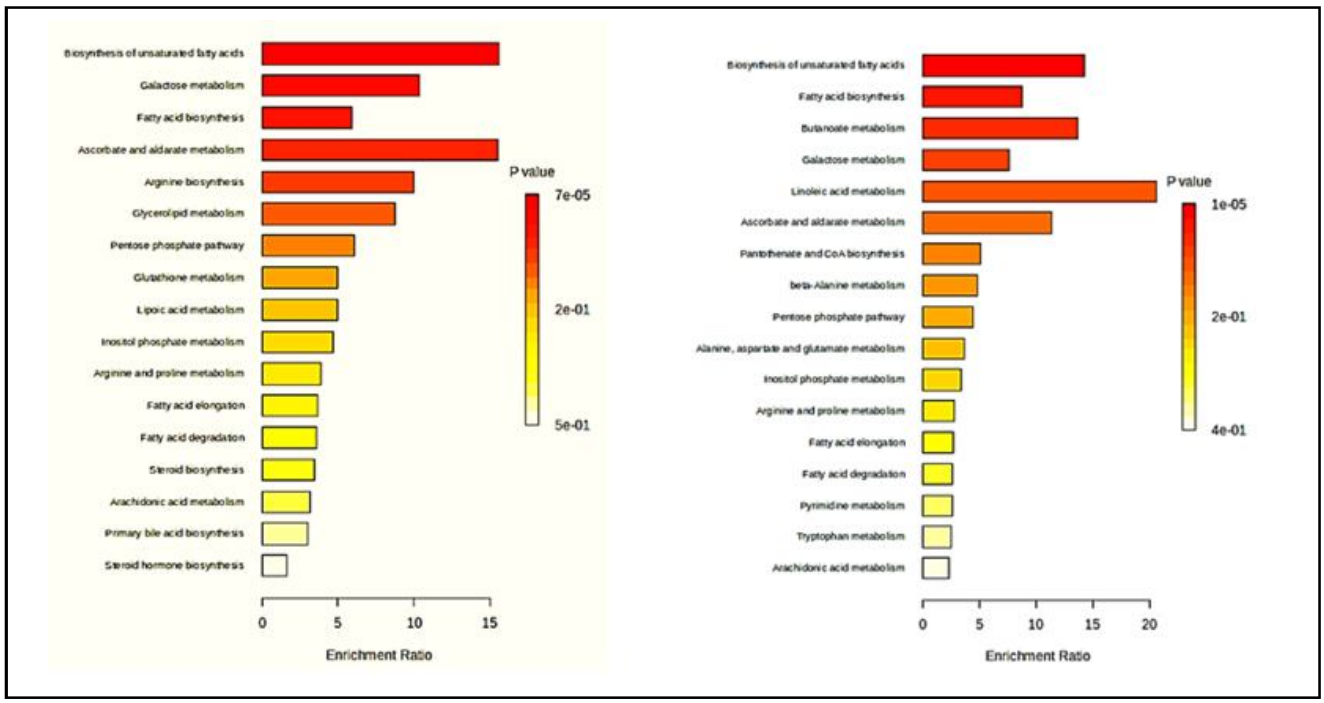

Figure 5e: Metabolic enrichment pathway analysis of CO5 leaves; 5f: Metabolic enrichment pathway analysis of Mash 1008 leaves.

4. Discussion

Mungbean yellow mosaic virus (MYMV) posed a significant threat to crop productivity by affecting plant health and yield. Understanding the biochemical and metabolic basis of resistance in plants is crucial for developing virus-resistant cultivars. Advances in metabolomics, particularly gas chromatography-mass spectrometry (GC-MS), have enabled the identification of compounds associated with plant defense mechanisms. This study explored the metabolic differences between resistant (Mash 1008) and susceptible (CO5) blackgram cultivars to understand the role of specific metabolites in YMD resistance. The research focused on profiling the diversity of metabolites in seeds, roots, and leaves of both resistant and susceptible cultivars. Further, based on the mining of the literature attempts

were made to identify the role of unique compounds with potential antiviral activity. By integrating normalization and correlation analysis, the study aimed to uncover biochemical interconnections and to elucidate resistance pathways.

In our study, the presence of unique metabolites in RC-Mash 1008 seeds, included campesterol, rhamnose, asperuloside, hentriacontonic acid, pyroglutamic acid, and gamma-sitosterol, highlights their potential role in plant defense. The sterol biosynthesis pathway progresses through key intermediates such as squalene, cycloartenol, and 24-methylene cycloartenol, ultimately leading to the formation of β-sitosterol, campesterol, and stigmasterol. Campesterol, a key component of the sterol biosynthesis pathway, contributes to antiviral resistance by participating in membrane stability and immune signaling. In the context of groundnut bud necrosis virus (GBNV) management, Sangeetha *et al*. (2021) reported that molecular modeling and docking studies identified squalene and ganoderic acid-A as potent inhibitors of the GBNV coat protein. *In vitro* assays demonstrated that squalene significantly reduced viral lesion size and titre in cowpea plants under controlled conditions, suggesting its potential as an eco-friendly antiviral agent.

Furthermore, previous studies reinforce the importance of specific metabolites in antiviral resistance. Niresh *et al*. (2024) identified elevated levels of norvaline, 10-eicosane, and campesterol in MYMV-resistant blackgram (Mash 114), linking these compounds to enhanced plant defense. Similarly, Manasseh *et al*. (2023) reported the predominance of oxyproline (pyroglutamic acid) in Potato virus Y (PVY) -resistant potato cultivar Premier Russet, emphasizing their antiviral properties. These findings collectively underscore the significance of sterol biosynthesis and secondary metabolites in conferring resistance against plant viral pathogens.

The study identified the metabolites methyl oleate, theophylline, lauric acid, and cysteine from Mash-1008 roots. The antiviral properties of theophylline have been well documented by Kurtzman *et al*. (1960), demonstrating its ability to inhibit tobacco mosaic virus (TMV) replication in tobacco, even at low concentrations. Yuan *et al*. (2024) observed that sugarcane mosaic virus (SCMV) infection in maize led to an increase in papain-like cysteine protease (PLCP) activity, particularly through the upregulation of Corn Cysteine Protease 1 (CCP1), which was shown to enhance resistance to SCMV. This aligns with our findings, as the presence of cysteine in Mash 1008 roots suggests a potential mechanism through which this cultivar may mount a stronger defense response. The biochemical composition of Mash 1008 blackgram leaves suggested a potential role in plant defense mechanisms, particularly against viral pathogens. The presence of linoleic acid in Mash 1008 is of particular interest, as previous studies by Librán-Pérez *et al*. (2019) and Lin *et al*. (2023) demonstrated that oleic acid, palmitic acid, and linoleic acid contributed to antibacterial activity against the growth of *Xanthomonas citri* subsp. *Citri* elicits induced systemic resistance (ISR) in plants. Beyond fatty acids, other metabolites have been implicated in antiviral activity. The presence of morpholine in Mash 1008 is noteworthy, as Zeng *et al*. (2024) synthesized morpholine-thiadiazole chalcone derivatives, with the sulfur-containing compound S14 from the natural product chalcone showing superior antiviral activity against tobacco mosaic virus (TMV) in tobacco leaves using a bioactivity test. Given this, it is plausible that morpholine in Mash 1008 could contribute to plant defense, although further studies are required to determine its precise role *in vivo*.

Additionally, hippuric acid, identified in Mash 1008, has been explored for its antiviral properties. According to Noha *et al*. (2021), hippuric acid influenced tomato mosaic tobamovirus (ToMV) replication, rather than acting as a direct virucidal agent, which was detected through cytotoxicity assays by observing local lesions on *Datura metal*, as well as infectivity assays on tomato plants. Although it exhibited weak inhibition at different concentrations (5, 10, 15, 20 ppm) in tomato plants inoculated with ToMV, it resulted in very low virus concentration and disease severity at 15 ppm, suggesting that it plays a role in limiting viral spread. These findings supported the hypothesis that hippuric acid contributes to plant defense through mechanisms other than direct viral neutralization.

Lipid metabolism appears to be intricately linked to plant defense mechanisms, as demonstrated by Kachroo *et al*. (2008). Their study using bean pod mottle virus (BPMV) vectors to silence stearoyl-acyl carrier protein-desaturase (SACPDs) in soybean plants led to decreased 18:1 oleic acid level, higher stearic acid accumulation, and increased salicylic acid (SA) production using gene silencing mechanism. These biochemical shifts were associated with spontaneous cell death lesions and constitutive expression of pathogenesis-related genes, further reinforcing the relationship between fatty acid metabolism and immune signaling.

Previous studies have shown that arachidonic acid (AA) signaling plays a significant role in plant defense. Rozhnova *et al*. (2003) observed suppression of tobacco mosaic virus (TMV) multiplication by 90 to100% upon AA treatment at concentrations ranging from 10{ y to 10{ w M, with 10{ x M being the optimal concentration in leaf disc assay, demonstrating the effectiveness of AA as a natural antiviral agent. Notably, the induced resistance persisted for at least two weeks, indicating the potential for AA to provide long-lasting protection against viral infection.

In contrast, CO5 showed elevated levels of metabolites such as uridine, juniperic acid, batyl alcohol, docosahexaenoic acid, fructofuranose, chiro-inositol, malonic and rosiridin, suggesting their association with susceptibility-related pathways that may facilitate viral replication and spread. Similarly, watermelon fruit and leaf infection with cucumber green mottle mosaic virus (CGMMV) significantly increased glucose, fructose, and sucrose levels were identified through the isobaric tags for relative and absolute quantitation (iTRAQ) technique (Li *et al*., 2018), which may contribute to viral replication and susceptibility.

Furthermore, Baur *et al*. (1967) examined malonic acid as a respiration inhibitor in TMV infected *Nicotiana tabacum*, targeting succinate dehydrogenase in the tricarboxylic acid cycle (TCA) using a differential respirometer. TMV infection altered glucose metabolism, increasing reliance on respiration.

This study highlights the importance of key metabolic pathways in plant response to pathogen infection. Pathways involved in lipid metabolism, energy production, and amino acid metabolism such as unsaturated fatty acid biosynthesis, the pentose phosphate pathway, the citric acid cycle, galactose metabolism, and arginine metabolism were associated with enhanced defence and stress resilience in both CO5 and Mash 1008. In contrast, dysregulation of pathways like steroid hormone synthesis, arachidonic acid metabolism, and cytochrome P450-mediated drug metabolism was linked to increased susceptibility.

Studies have shown varying amino acid responses in virus-infected tomato plants. ToMV-infected leaves exhibited a general reduction in amino acid levels (Lopez Gresa *et al*., 2010), whereas *P. syringae*-infected leaves showed elevated levels of specific amino acids (Perez-Garcia *et al*., 1998; Eason *et al*., 1996). However, glutamine/glutamate and asparagine/aspartate were notably increased in ToMV-infected leaves. Supporting these findings, Zhu *et al*. (2024) investigated the defense response of SMV-resistant soybean line Dongnong 93-046 against the SMV N1 strain using transcriptomic and metabolomic analyses. Their study identified 41,189 differentially expressed genes (DEGs), with 9,809 meeting significance thresholds. KEGG pathway enrichment revealed key resistance-related pathways, including plant–pathogen interaction, linoleic acid metabolism, MAPK signaling, and hormone signal transduction.

Additionally, the NMR-based metabolomics data derived by Maravi *et al*. (2022) and Shalitin *et al*. (2000) revealed increased concentrations of α- and β-glucose in both the apoplast and symplast in response to mungbean yellow mosaic India virus (MYMIV) infection in mungbean leaves, indicating a shift in glucose utilization. Despite of this, the production of phenolic intermediates, which were strongly induced by MYMIV in mungbean, remained unaffected. This suggested that the elevated levels of carbohydrates such as sucrose and fructose in MYMIV infected leaves likely to serve as energy sources for viral replication The increased level of various metabolites, including sucrose, fructose, glycine, tyrosine, asparagine, ketoglutaric acid, pyruvate, arabinose, p-coumaric acid, malate, and salicylate was observed in MYMIV infected mungbean leaves (Maravi *et al*., 2022). These evidences further underscore the complex metabolic alterations induced during infection in SC CO5.

This study unraveled the hidden biochemical arsenal that black gram cultivars deployed against mungbean yellow mosaic virus. Through meticulous normalization and correlation analyses, the dynamic interplay of these compounds was brought to light, revealing their critical contributions to resistance pathways. These findings not only deepened the understanding of plant-virus warfare but also laid the groundwork for revolutionizing crop protection. By harnessing the power of these natural defenders, this research paved the way for breeding virus-resistant crops and unlocking a future of resilient, sustainable agriculture, where plants thrive and pathogens falter.

5. Conclusion

This study illuminated the intricate biochemical mechanisms underlying resistance to mungbean yellow mosaic virus (MYMV) in black gram cultivars. The identification of key metabolites such as myo-inositol, methyl linolenate, ribose, and arachidonic acid showcases the pivotal role of metabolic pathways in strengthening plant defenses. The use of advanced metabolomic techniques has enabled a deeper understanding of how specific compounds contribute to resistance, revealing a complex network of interactions that fortify the plants immune response. The elevated levels of metabolites such as uridine, juniperic acid, batyl alcohol, and chiro-inositol in CO5 across different tissues suggested their potential involvement in susceptibility-related pathways, highlighting key metabolic differences associated with disease susceptibility. By unveiling these hidden biochemical arsenals, the study enhances our understanding of plant-pathogen interactions and provides valuable insights for developing virus-resistant cultivars. This research lays the foundation for future advancements in crop protection and highlights the potential for sustainable, resilient agriculture. As we harness these natural defense mechanisms, the future of crop breeding looks for promising resources, where plants are empowered to withstand viral threats, ensuring food security and ecological balance.

Acknowledgments

Support from Department of Plant Pathology and Department of Plant Biotechnology, Tamil Nadu Agricultural University, Coimbatore, is greatly acknowledged.

Conflict of interest

The authors declare no conflicts of interest relevant to this article.

References

Basak, J.; Kundagramy, S.; Ghose, T. K. and Pal, A. (2005). Development of yellow mosaic virus (YMV) resistance-linked DNA-marker in *Vigna mungo* from population segregating for YMV reaction. Molecular Breeding, **14**:375-383.

Baur, J. R.; Halliwell, R. S. and Langston, R. (1967). Effect of *Tobacco mosaic virus* infection on glucose metabolism in *Nicotiana tabacum* L. var. Samsum II: Investigation of malonic acid inhibition on respiration. Virology, **32**(3):413-415. https://doi.org/10.1016/0042-6822(67)90292-9

Bhawana Sharma; Shiv Charan Sharma and Afroz Alam (2021). Phytochemical screening and GC-MS analysis of *Tamarindus indica* L. (Angiosperms: Fabaceae). Ann. Phytomed., **10**(1):215-221. http://dx.doi.org/10.21276/ ap.2021.10.1.23

Dhanushkodi Vellaiyan; A. Thanga Hemavathy.; R. Anitha.; S. Sangeetha, S.; Shenbagavalli.; Noorjehan A.K.A. Hanif.; K. Yamunarani.; R. Nageswari.; S. Rathika and D. Amirtham (2024). A comprehensive review on a potential medicinal plant, *Vitex negundo* L. Ann. Phytomed., **13**(1):407-416. http://dx.doi.org/10.54085/ap.2024.13.1.41.

Eason, J. R.; O'Donoghue.; E. M. and King, G. A. (1996). Asparagine synthesis and localization of transcripts for asparagine synthetase in the tips of harvested asparagus spears. Journal of Plant Physiology, **149**:251-256.

Gupta, S. and Parihar, A. K. (2015). Broadening the genetic base of pulse crops. Pulses: Challenges and Opportunities, pp:86-101.

Gupta, S.; Das, A.; Pratap, A. and Gupta, D. S. (2021). Urdbean. In: The Beans and the Peas, 33:54. https://doi.org/10.1016/B978-0-12-82145 0-3.00014-7.

Jegadeesan, S.; Raizada, A.; Dhanasekar, P. and Suprasanna, P. (2021). Draft genome sequence of the pulse crop blackgram (*Vigna mungo* (L.) Hepper) reveals potential R-genes. Scientific Reports, **11**:11247. https://doi.org/10.1038/s41598-021-90683-9

Kachroo, A.; Fu, D-Q.; Havens, W.; Navarre, D.; Kachroo, P. and Ghabrial, S. A. (2008). An oleic acid–mediated pathway induces constitutive defense signaling and enhanced resistance to multiple pathogens in soybean. Molecular Plant-Microbe Interactions, **21**(5):564-575. https://doi.org/10.1094/MPMI-21-5-0564

K.S. Vijai Selvaraj.; T. Prabha.; J. Karthikeyan.; C. Indu Rani.; P. Irene Vethamoni and A. Bharathi (2024). Harnessing nature's arsenal: A comprehensive review of phytomedicine approaches in Monkeypox treatment. Ann. Phytomed., **13**(2):23-32. http://dx.doi.org/10.54085/ap.2024.13.2.3.

Kumudini, B. S.; Jayamohan, N. S.; Patil, S. V. and Govardhana, M. (2018). Primary plant metabolism during plant pathogen interactions and its role in defense. Plant Metabolites and Regulation Under Environmental

Stress, pp:215-229. Academic Press. https://doi.org/10.1016/B978-0-12-812689-9.00011-X

Kurtzman, R. H.; Hildebrandt, A. C.; Burris, R. H. and Riker, A. J. (1960). Inhibition and stimulation of tobacco mosaic virus by purines. *Virology,* **10**(4):432-448. https://doi.org/10.1016/0042-6822(60)90127-6.

Li, L. M.; Li, X.; Zhao, X. X.; Mao, H.; Sun, J. H. and Wu, Y. H. (2018). The relationships between sugar metabolism and blood-flesh of watermelon infected with Cucumber green mottle mosaic virus. Journal of Plant Protection, **45**(3):447-454.

Librán-Pérez, M.; Pereiro, P.; Figueras, A. and Novoa, B. (2019). Antiviral activity of palmitic acid *via* autophagic flux inhibition in zebrafish (*Danio rerio*). Fish and Shellfish Immunology, **95**:595-605. https://doi.org/10.1016/j.fsi.2019.10.055

Lin, H.; Liang, Y. and Kaliaperumal, K. (2023). Linoleic acid from the endophytic fungus *Diaporthe* sp. HT-79 inhibits the growth of *Xanthomonas citri* subsp. *citri* by destructing the cell membrane and producing reactive oxygen species (ROS). Pesticide Biochemistry and Physiology, **192**:105423. https://doi.org/10.1016/j.pestbp.2023.105423

Llave, C. (2016). Dynamic cross-talk between host primary metabolism and viruses during infections in plants. Current Opinion in Virology, **19**:50-55.

López-Gresa, M. P.; Maltese, F.; Bellés, J. M.; Conejero, V.; Kim, H. K. and Choi, Y. H. (2010). Metabolic response of tomato leaves upon different plant–pathogen interactions. Phytochemical Analysis, **21**:89-94.

Manasseh, R.; Berim, A.; Kappagantu, M.; Moyo, L.; Gang, D. R. and Pappu, H. R. (2023). Pathogen-triggered metabolic adjustments to *Potato virus Y* infection in potato. Frontiers in Plant Science, **13**:1031629. https://doi.org/10.3389/fpls.2022.1031629

Maravi, D. K.; Kumar, S. and Sahoo, L. (2022). NMR-based metabolomic profiling of mungbean infected with Mungbean Yellow Mosaic India Virus. Applied Biochemistry and Biotechnology, **194**:5808-5826. https://doi.org/10.1007/s12010-022-04074-5

Narmadha Devi, A.; Sundharaiya, K.; Rajanga, J.; Gnanasekaran, M.; Vijayasamundeeswari, A. and M. Kabilan (2024). Biochemical and phytochemical analysis of Yardlong bean (*Vigna unguiculata* (L.) Verdc. Subsp. *sesquipedalis*) using gas chromatography and mass spectroscopy (GC-MS). Ann. Phytomed., **13**(2):812-821. http://dx.doi.org/ 10.54085/ap.2024.13.2.83.

Niresh Kumar, S.; Satya, V K.; Renukadevi, P.; Malathi, V G.; Saranya N. and Thiyagu K (2024), Deciphering temporal metabolome dynamics in response to MYMV: Contrasting patterns in resistant and susceptible blackgram (*Vigna mungo* L. Hepper) cultivars, Journal of Agricultural and Food Chemistry, **72** (46):25620-25637 DOI: 10.1021/acs.jafc.4c06400

Noha.K. El Dougdoug.; Hala.K. El Shahat.; M.M. Amer.; W.A. El Dougdoug. and K.A. El Dougdoug, (2021), Action mechanism of synthesized nitrogen base analogues that inhibit tomato mosaic tobamovirus, Benha Journal of Applied Science, **42**:269-278

Patidar, M. and Sharma, H. (2017). Correlation and path coefficient studies in blackgram (*Vigna mungo* (L.) Hepper). Journal of Pharmacognosy and Phytochemistry, **6**:1626-1628.

Pérez-García, A.; Pereira, S.; Pissarra, J.; Gutiérrez, A. G.; Cazorla, F. M. and Salema, R (1998). Cytosolic localization in tomato mesophyll cells of a novel glutamine synthetase induced in response to bacterial infection or phosphinothricin treatment. Planta, **206**:426-434.

Peyraud, R.; Dubiella, U.; Barbacci, A.; Genin, S.; Raffaele, S. and Roby, D. (2017). Advances on plant-pathogen interactions from molecular toward systems biology perspectives. The Plant Journal, **90**(4):720-737. https://doi.org/10.1111/tpj.13429

Rajalakshmi, K.; Murugan, E.; Anand, G.; Renuka, R. and Ramamoorthy, V. (2024). Study on blackgram (*Vigna mungo* L. Hepper) genotypes for yield stability and Mungbean Yellow Mosaic Virus (MYMV) resistance. Electronic Journal of Plant Breeding, **15**(1):147-154. https://www.ejplantbreeding.org/index.php/EJPB/article/view/5025.

Raghunadha Reddy, G. (2024). Crop outlook reports of Andhra Pradesh - Blackgram. Centre for Agricultural and Rural Development Policy Research (CARP), Guntur, pp:1-6.

Rozhnova, N. A.; Gerashchenkov, G. A. and Babosha, A. V. (2003). The effect of arachidonic acid and viral infection on the phytohemagglutinin activity during the development of tobacco acquired resistance. Russian Journal of Plant Physiology, **50**:661-665. https://doi.org/10.1023/A:1025696325679.

Sangeetha B.; Krishnamoorthy AS.; Sharmila DJS.; Renukadevi P.; Malathi VG. and Amirtham D. (2021). Molecular modelling of coat protein of the Groundnut bud necrosis tospovirus and its binding with Squalene as an antiviral agent: *In vitro* and *in silico* docking investigations. Int J Biol Macromol., **189**:618-634. doi: 10.1016/j.ijbiomac. 2021. 08.143.

Shalitin, D. and Wolf, S. (2000). *Cucumber mosaic virus* infection affected sugar transport in melon plants. Plant Physiology, **123**(2):597–604.

Singh, D. P., Singh, B. B., and Pratap, A. (2016). Genetic improvement of mungbean and urdbean and their role in enhancing pulse production in India. Indian Journal of Genetics, **76**(4):550-567. https://doi.org/10.5958/0975-6906.2016.00072.9.

Vaishnavi, B.A.; Venkatesan, K.; Senthil, N.; Mohanalakshmi, M.; Paranitharan, V.; Thamaraiselvi, S.P. and Vellaikumar, S. (2024). Variation in the volatile oil composition and antioxidant activity of Zingiberaceae: A comparative investigation. Ann. Phytomed., **13**(1):1008-1018. http://dx.doi.org/10.54085/ap.2024.13.1.109.

Weng, J.; Lynch, J. H.; Matos, J. and Dudareva, N. (2021). Adaptive mechanisms of plant specialized metabolism connecting chemistry to function. Nature Chemical Biology, **17**:1037-1045.

Yuan, W.; Chen, X.; Du, K.; Jiang, T.; Li, M.; Cao, Y.; Li, X.; Doehlemann, G.; Fan, Z.; and Zhou, T. (2024). NIa-Pro of *sugarcane mosaic virus* targets Corn Cysteine Protease 1 (CCP1) to undermine salicylic acid-mediated defense in maize. PLoS Pathogens, **20**(3):1012086. https://doi.org/10.1371/journal.ppat.1012086.

Zeng, W.; Sun, Z.; Zhang, Y.; Hu, Y.; Zhou, Q.; Qiu, Y.; Li, J. and Xue, W. (2024). New chalcone derivatives containing morpholine-thiadiazole: Design, synthesis, and evaluation against *tobacco mosaic virus*. Fitoterapia, **179**:106272. https://doi.org/10.1016/j.fitote.2024.106272.

Zhu, H.; Li, R.; Fang, Y.; Zhao, X.; Teng, W.; Li, H. and Han, Y. (2024). Weighted gene co-expression network analysis uncovers critical genes and pathways involved in soybean response to *soybean mosaic virus*. Agronomy, **14**:2455. https://doi.org/10.3390/agronomy14112455.

Citation **R. Sariga, P. Renukadevi, S. Nakkeeran, I. Yesuraja, J. Ramalingam, A. Yuvaraja and S. Vellaikumar (2025). A comparative metabolome analysis of seed, root, and leaf of blackgram cultivars in response to Mungbean yellow mosaic virus (MYMV) infection reveals a unique signature profile for resistance. Ann. Phytomed., 14(1):1028-1042. http://dx.doi.org/10.54085/ap.2025.14.1.103.**